Green Chemistry

PAPER

View Article Online
View Journal | View Issue

Cite this: *Green Chem.*, 2025, **27**, 2220

High-strength, self-healable, transparent castor-oil-based waterborne polyurethane barrier coatings enabled by a dynamic acylhydrazone co-monomer†

Guowen Zhou,[a] Yunfeng Zhou,[a] Xiaoqian Zhang,[a] Zepeng Lei*[b] and Xiaohui Wang *[a]

Castor oil-based waterborne polyurethanes (CWPUs) are recognized as sustainable polymers sourced from renewable materials. However, these polymers often exhibit suboptimal mechanical properties and lack reprocessability due to their soft backbones and irreversible crosslinking structures. Herein, we synthesized a novel rigid diol (VSD) featuring dynamic acylhydrazone covalent bonds, which remain stable even in aqueous environments and can contribute additional hydrogen bonding sites, through the condensation reaction of commercially available succinohydrazide with lignin-derived vanillin. VSD was subsequently introduced into the CWPU system to form colorless and transparent CWPU-VSD films, which exhibited self-healable and reprocessable properties due to the dynamic nature of the acylhydrazone bond. By adjusting the ratio of VSD (the 'hard' section) to castor oil (the 'soft' section), the mechanical properties of CWPU-VSDs were finely tuned, achieving an optimal tensile strength of 33.9 MPa. Moreover, the application of this CWPU as a paper-based functional coating was explored. The coated paper exhibited excellent water and oil resistances, low water vapor permeability, good recyclability and biodegradability, suggesting a promising approach for the development of multifunctional and sustainable paper-based barrier coatings.

Received 2nd December 2024,
Accepted 24th January 2025

DOI: 10.1039/d4gc06103a

rsc.li/greenchem

Green foundation

1. A molecular design strategy is proposed to enhance the mechanical properties and self-healing ability of castor oil-based waterborne polyurethanes (CWPUs) by introducing sustainably rigid diols containing dynamic acylhydrazone bonds.
2. This CWPU coating for paper substrates exhibits significant environmental and barrier advantages over some biomass-based coatings, establishing a pathway toward environmentally friendly alternatives in the paper-based packaging industry.
3. Future research effort could focus on the preparation of fully bio-based CWPUs, further enhancing the natural degradability of coatings by increasing the bio-based content.

1. Introduction

Polyurethane (PU), typically synthesized through the polyaddition between polyols and isocyanates, has emerged as one of the most versatile polymeric materials globally, with applications in various fields such as coatings, adhesives, foam materials, and elastomers.[1] In light of strict environmental regulations, the development of waterborne polyurethanes (WPUs) that utilize water as the primary solvent has garnered significant attention, as it avoids the use of volatile organic compounds (VOCs) typically associated with conventional solvent-based polyurethane production.[2,3] Moreover, the polyols and isocyanates used in PU synthesis are traditionally derived from fossil fuels, which are increasingly considered unsustainable. Consequently, the pursuit of renewable resources for the synthesis of WPUs is becoming both urgent and important.

Castor oil (CO) is the only natural vegetable oil containing hydroxyl groups that can be directly used as a polyol for the preparation of sustainable WPUs without further modification.[4,5] However, the flexible long fatty acid chains in

[a]State Key Laboratory of Pulp and Paper Engineering, South China University of Technology, Guangzhou 510640, China. E-mail: fewangxh@scut.edu.cn
[b]Department of Chemistry, University of Colorado Boulder, Boulder, Colorado 80309, USA. E-mail: Zepeng.lei@colorado.edu

†Electronic supplementary information (ESI) available. See DOI: https://doi.org/10.1039/d4gc06103a

CO tend to compromise the tensile strength of the resultant WPU.[6] Previous studies have shown that incorporating rigid cyclic structures in the backbone of polymer chains is a straightforward and effective way to improve mechanical strength.[7–10] For example, Zhang and co-workers enhanced the tensile strength of CO-based WPU (CWPU) from 9.5 to 22.3 MPa by integrating octahydro-2,5-pentalenediol, a moiety with two parallel rigid cyclopentane rings made from citric acid.[9] In another work, a sustainable L-tyrosine derived cyclic dipeptide (L-CD) containing a rigid benzene ring and abundant hydrogen bond-binding sites was incorporated into the network polymer. The tensile strength of the resulting CWPU films reached 29.6 MPa.[10] However, the inherent triglyceride structure of CO leads to permanently linked thermoset polyurethanes that are not reprocessable or recyclable after curing.[7,11,12] Once damaged or beyond their service life, these materials would inevitably generate a significant amount of plastic waste.

To address these challenges, dynamic covalent chemistry provides a promising solution. It has made substantial progress in developing novel network polymers,[13,14] including crosslinked PUs.[15] Typical dynamic linkages such as disulfide bonds,[16] Diels–Alder bonds,[17] diselenide bonds,[18] boronic ester bonds,[19] and imine bonds[20] have been extensively applied in this field. Those dynamic covalent bonds within the network structure could reversibly break and recombine under certain external stimuli to endow the crosslinked materials with self-healing, reprocessing, and recycling capabilities. However, the aqueous medium largely limited the selection of dynamic bonds.[21] For example, due to the instability of imine bonds in water, self-healing polyurethanes using imines were predominately solvent-based.[22–24] Most reported WPUs containing dynamic linkages were based on disulfide bonds,[7,25,26] but this molecular design usually resulted in a dark yellow appearance and reduced transparency in WPU films. Therefore, it is significantly urgent to explore more feasible approaches for the construction of dynamic bonds in CWPUs with a unique combination of high mechanical performance, good transparency, and self-healing properties.

Herein, we report a highly transparent CWPU with enhanced mechanical strength and toughness, as well as self-healing and reprocessable properties *via* incorporating reversible acylhydrazone bonds. Specifically, we synthesized a novel rigid diol (VSD) containing dynamic acylhydrazone bonds for CWPU systems through the condensation of commercially available succinic dihydrazide and vanillin, a lignin-derived biobased monomer with a phenyl ring in its structure. The acylhydrazone bond offers greater stability in water compared to the imine bond and introduces additional hydrogen bonding sites.[27,28] The presence of two rigid phenyl rings in VSD, the "hard" segment, allows for the fine-tuning of the mechanical properties of CWPU by adjusting the ratio of VSD to CO, the "soft" segment. Furthermore, we explored the application of this CWPU dispersion as a functional coating for paper substrates, revealing its potential as a sustainable solution for the development of attractive paper-based barrier coatings.

2. Experimental section

2.1. Materials

Castor oil (CO, OH number: 177–187 mg KOH per g) was purchased from Damao Chemical Reagent Factory (Tianjin, China). Vanillin (99%) and succinic dihydrazide (97%) were purchased from Aladdin Reagents. Isoflurone diisocyanate (IPDI, 99%), dimethylol butanoic acid (DMBA, 99%), triethylamine (TEA, >99%) and dibutyltin dilaurate (DBTDL, 95%) were purchased from Macklin Biochemical Co., Ltd (Shanghai, China). *N*,*N*-Dimethylacetamide (DMAc), acetone, and ethanol were purchased from Guangzhou Chemical Reagents. All materials were used without further purification.

2.2. Methods

2.2.1 Synthesis of reversible covalent bond acylhydrazone diol. Succinic dihydrazide (7.53 g, 0.0500 mol) and vanillin (15.37 g, 0.100 mol) were completely dissolved in deionized water (50 mL) and ethanol (50 mL), respectively. Then, the ethanol solution of vanillin was slowly added to the aqueous solution of succinic dihydrazide and the mixture was allowed to react under mechanical stirring for 3 h at 70 °C. After filtration and purification (washing with water and ethanol), the white powder product was dried at 50 °C until a constant mass was achieved. The white product was named VSD, and the yield was 93.20%.

2.2.2. Preparation of CWPUs. DMBA (0.81 g, 5.5 mmol) and VSD monomers were initially dissolved in a small amount of DMAc. Firstly, IPDI (2.9 g, 13 mmol) and DBTDL (5 μL) were mechanically stirred in a three-neck round bottom flask for 10 min at 30 °C. Then, the mixture containing castor oil and DMBA was added and stirred at 120 rpm and reacted at 70 °C for 2 h to prepare the prepolymer. Next, VSD used as chain extenders was introduced into the reaction and continued to react under stirring for 2 h at 70 °C. The molar ratios of the total OH groups (provided by CO and monomer VSD), the NCO group in IPDI and the OH group in DMBA were kept 1 : 1.75 : 0.74, and the molar ratios of the OH groups in CO and VSD varied from 10 : 0 to 9 : 1, 8 : 2 and 7 : 3, which were named CWPU, CWPU-VSD10, CWPU-VSD20 and CWPU-VSD30, respectively. Throughout the reaction, the viscosity was adjusted by adding an appropriate amount of acetone. When the mixture was cooled down to room temperature, TEA was slowly added to neutralize the carboxyl group of DMPA with a 1 : 1 molar ratio. After 0.5–1 h, 25 mL of deionized water was added for emulsification under high-speed stirring of 1100 rpm for 1 h. Finally, acetone was removed by rotary evaporation to obtain a CWPU dispersion with a solid content of approximately 25 wt%. The formulations of samples are detailed in Table 1.

2.2.3. Preparation of CWPU films. The dispersions were poured into smooth molds and dried at 40 °C to remove most of the water, and then they were further dried at 80 °C for 12 h to obtain CWPU films with a thickness of 0.4 ± 0.05 mm.

2.2.4. Preparation of coated papers. A certain amount of CWPU-VSD30 dispersions was uniformly coated on 20 × 15 cm^2

Table 1 The formulation details and properties of the CWPU dispersions

Samples	Molar ratio				Size (nm)	Zeta potential (mV)	Viscosity (mPa s)
	–NCO (IPDI)	–OH (CO)	–OH (DMBA)	–OH (VSD)			
CWPU	1.75	1	0.74	—	168.0	−50.2	18.5
CWPU-VSD10	1.75	0.9	0.74	0.1	89.2	−42.1	17.2
CWPU-VSD20	1.75	0.8	0.74	0.2	56.8	−45.7	14.5
CWPU-VSD30	1.75	0.7	0.74	0.3	25.1	−42.5	10.7

base paper with a basis weight of 78 g m^{-2} by using a rod coating machine and dried at 60 °C for 10 min in an oven.

2.3. Characterization

A Fourier transform infrared (FTIR) spectrometer, Vector 70 from Bruker, Germany, with a wavelength range of 400–4000 cm^{-1} and 16 or 32 scans was employed to characterize the samples. The ^1H NMR spectrum of the VSD monomer was analyzed using a Bruker AVANCE III NMR spectrometer (400 MHz) with dimethyl sulfoxide (DMSO-d6) as a deuterated reagent. The transmittance tests of films were performed using a UV/VIS spectrophotometer (UV-1900). The surface of the paper and coated paper was observed with a Hitachi SU5000 VP-SEM, and samples were sputter-coated with gold before testing.

The average particle size and zeta potential of the dispersions were tested on dynamic light scattering using the DLS nanometer particle size analyzer at room temperature. Before testing, the dispersions were diluted to about 0.01 wt% with distilled water. The viscosity values of dispersions were obtained using a NDJ-1 rotary viscometer at 25 °C. The Turbiscan stability index (TSI) curves of dispersions were obtained using the Turbiscan LabExpert with scanning every 40 μm at 50 °C. The tensile properties of films were determined using an Instron 5565 tensile tester with a 30 mm gauge length (dimensions of 50 × 5 mm) at a tensile velocity of 50 mm min^{-1}. The thickness of the samples was measured with a digital caliper. For each sample, three parallel specimens were tested.

The glass transition temperature (T_g) of film samples was measured using differential scanning calorimetry (DSC) with a TA DSC Q20. All samples were first heated from 30 to 100 °C, then cooled to −50 °C and later heated to 140 °C at a rate of 10 °C min^{-1}. The thermogravimetric analysis (TGA) curves and thermogravimetric differential (DTG) curves were measured using a Netzsch TG209F1 thermogravimetric (TG) analyser with a heating rate of 20 °C min^{-1} in nitrogen gas.

2.4. Water contact angle, hygroscopicity, gel fraction and barrier tests

The water contact angle of film samples was tested on a ZJ-7000 optical contact angle tester (China). The hygroscopicity was measured by submerging film samples in water for a specific time followed by testing the weight increase rate.

The gel fraction (G_f) values of film samples were calculated as follows: about 0.1 g (m_0) of sample was placed in DMF and immersed at room temperature for 24 h. Then the solvent was removed from the surface of the sample using filter paper and the sample was dried in a vacuum oven at 80 °C to constant weight as m_1. The G_f is calculated according to the following equation:

$$G_f = m_1/m_0 \times 100\%. \quad (1)$$

The water absorption of coated paper was determined as the Cobb 60 value, tested using a Cobb sizing tester (LB-K100, China) following the Chinese Standard GB/T 1540-2002. The water vapor transmission rates (WVTR) were measured at 30 °C with relative humidity (90 ± 1%) using a WVTR tester (PERMATRAN 3/34G, America).

2.5. Biocompatibility and degradability tests

Biocompatibility testing of samples was evaluated using bundled mouse fibroblast (NIH-3T3) cells and the results were assessed using the CCK8 assay. Firstly, NIH-3T3 cells were inoculated into a 96-well plate with 1.0×10^4 cells per well. Then, paper samples were cut into specimens with specific sizes. After being disinfected with a 75% ethanol solution, exposed to ultraviolet light for 30 min, and washed 3 times with sterile PBS buffer (pH of 7.4), samples were cultivated with NIH-3T3 cells in the cell culture medium at 37 °C. After 24 h, the cytotoxicity of samples was assessed using fluorescence microscopy, where live and dead cells were labeled green and red, respectively. The culture medium containing only cells was used as a control. Three sets of parallel tests were performed for each group of samples.

The paper and coated paper were cut into sheets of the same size and then buried in natural soil at a depth of 5 cm to test the biodegradability. Samples were taken out periodically for observation and the weight change of the samples with time was recorded.

3. Results and discussion

3.1. Preparation and characterization of VSD and CWPU dispersions

A rigid diol monomer, VSD, was prepared *via* a one-step condensation reaction of succinic dihydrazide and vanillin (Fig. S1a†). In the FTIR spectra (Fig. S1b†), the absorption peak at 1670 cm^{-1} attributed to the aldehyde group of vanillin completely disappeared, while peaks at 1650 and 1604 cm^{-1} attributed to the stretching vibrations of C═O and C═N

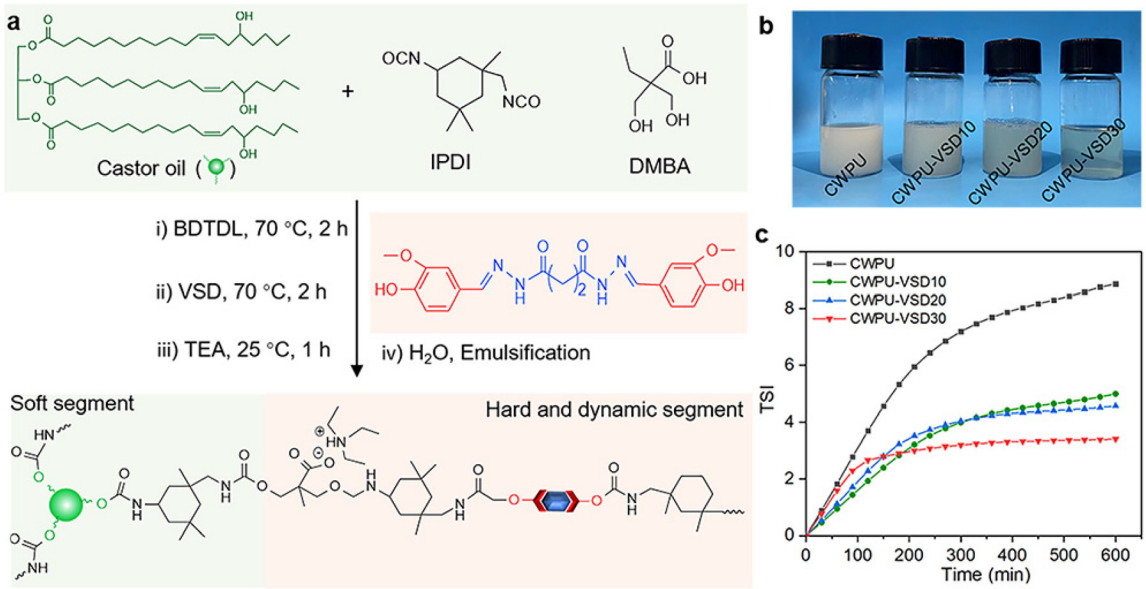

Fig. 1 (a) Synthetic routes employed for the preparation of VSD/castor-oil-based WPU dispersions. (b) Photo showing the appearance of CWPU dispersions. (c) The curves of TSI over time under the isothermal condition of 50 °C.

groups were observed in the curve of VSD. Furthermore, the ^{1}H NMR spectrum (Fig. S1c†) showed peaks at 11.25 and 11.10 ppm related to protons of –CONH–, and a peak at 9.45 ppm was assigned to –OH. Additionally, peaks at 8.05 and 7.88 ppm related to the hydrogen protons of –CH═N– were observed, confirming the successful synthesis of the VSD monomer.

With the introduction of VSD into the CWPU system (Fig. 1a), the appearance of the resulting dispersions changed significantly from milky white to translucent under blue light, as illustrated in Fig. 1b. This change was mainly caused by the difference in the particle size, which decreased from 168.0 nm to 25.1 nm as the VSD (hard segment) content increased (Fig. S2†). Furthermore, the stability of the dispersions was assessed using the Turbiscan Stability Index (TSI) calculated using Turbiscan software, and the results are displayed in Fig. 1c. A lower TSI value indicated a more stable dispersion, suggesting that the incorporation of VSD would help to improve the stability of CWPUs. All emulsion samples were centrifuged at 2000 rpm for 30 min (referring to the lotion centrifugal stability test standard), and no precipitation or coagulation was observed, indicating that they could be stored for extended periods.

3.2. Preparation and characterization of CWPU films

After conventional solvent-casting, stable emulsion samples produced colorless and transparent films with up to 90% transmission (Fig. 2a). Notably, CWPU-VSD10, CWPU-VSD20 and CWPU-VSD30 exhibited good ultraviolet (UV) resistance in the wavelength range of 300–350 nm, which can be attributed to the presence of –C═N– bonds and aromatic groups within the network structure that effectively absorb UV light.[29] The FT-IR spectra of oven-dried film samples are shown in Fig. 2b. The disappearance of the peak at 2270 cm^{-1} indicates complete consumption of the –NCO in IPDI. All samples exhibit a broad peak at 3200–3500 cm^{-1}, attributed to the –NH asymmetric stretching vibration of the carbamate bond, confirming the successful preparation of polyurethane. Importantly, the vibrational peak of –C═N– at 1607 cm^{-1} appeared in CWPU-VSD samples and its absorption intensity increased gradually with the increase in the VSD monomer content.

Then, the mechanical properties of the films were investigated (Fig. 2c). It was found that the mechanical properties of films could be effectively tuned by adjusting the ratio of VSD ("hard" section) and castor oil ("soft" section). We attempted to further increase the VSD content, but the obtained films were too brittle to fully demold, making it impossible to collect detailed data. The tensile strength of samples significantly increased as VSD gradually replaced part of CO as the chain extender, accompanied by a decline in elongation at break. Specifically, the elongation at break of the CWPU film was 774% with a low tensile strength of 14.5 MPa, while the CWPU-VSD30 film exhibited a decreased stretchability of 220% with a high tensile strength of 33.9 MPa, superior to most of the reported castor-oil-based WPUs.[5,10,30,31] The notable mechanical strength of CWPU-VSD30 was further demonstrated using a thin sheet with a width of 1.5 cm and a thickness of 0.5 mm to lift a 5.9 kg water bucket, as displayed in Fig. 2d. For the improvement of tensile strength, we hypothesized that this could be attributed to two main reasons. On the one hand, the aromatic benzene structure directly enhanced the rigidity of the network, thus improving the stiffness of the film materials. On the other hand, due to the additional hydrogen bonding sites provided by VSD, the hydro-

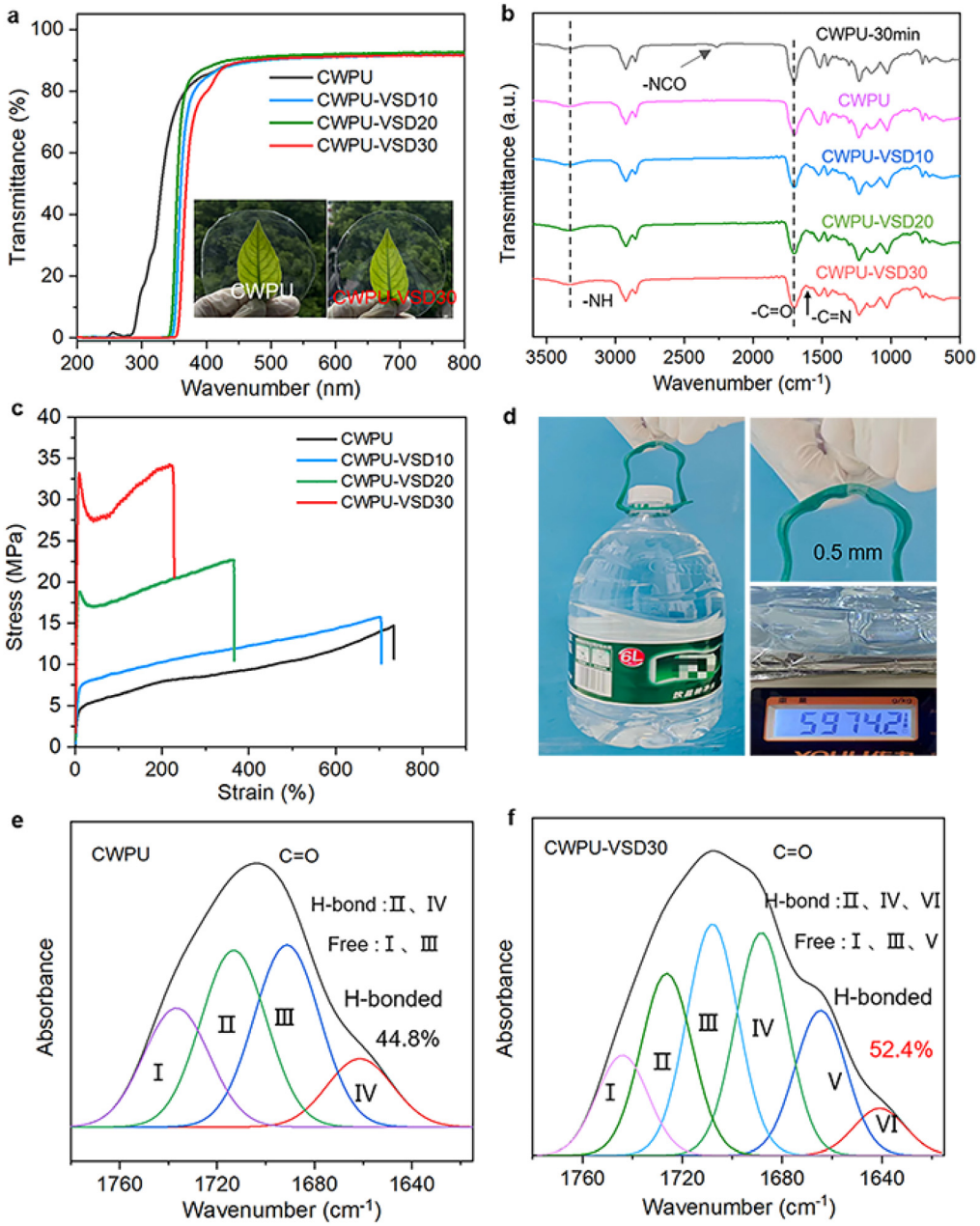

Fig. 2 (a) UV–vis transmittance spectra. Inset: photos of the CWPU and CWPU-VSD30 (colorless and transparent) films. (b) FTIR spectra of CWPU and CWPU-VSD samples. (c) Stress–strain curves of CWPU and CWPU-VSD films. (d) Photos showing that CWPU-VSD30 thin sheet can lift a weight of about 6 kg. Curve-fitting results of the carbonyl region in the FTIR spectra for (e) CWPU and (f) CWPU-VSD30.

gen bonding interactions within networks were enhanced. According to the literature reports,[7,32] the content of hydrogen bonds in WPUs can be determined by deconvolution of the C=O absorption band in the FTIR spectrum. As shown in Fig. 2e and f, the C=O region in CWPU and CWPU-VSD30 was deconvoluted into four and six subpeaks, respectively: I, III and V for free C=O, and II, IV and VI for H-bonded C=O of urethane, amide and ester groups. Quantitative analysis suggested that the ratio of H-bonded C=O in CWPU-VSD30 increased by 7.6% compared to CWPU, which would benefit the mechanical properties of the obtained films. In addition, the proportions of H-bonded C=O of samples increased slightly with increasing VSD content (Fig. S3†).

3.3. Thermophysical properties

DSC was used to analyze the thermal behavior of the above-mentioned films, as shown in Fig. 3a. There are no melting or crystallization transition peaks and only one glass transition temperature (T_g), indicating that these samples are amorphous. As the proportion of hydroxyl groups in VSD to those in

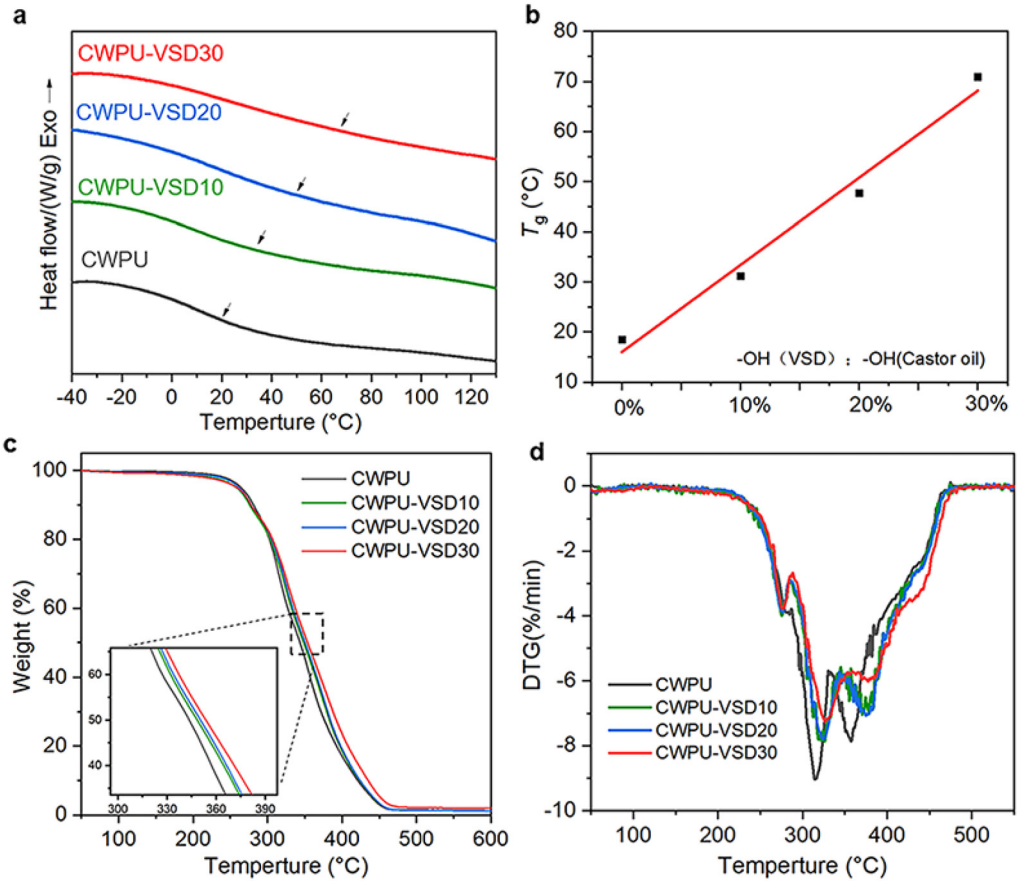

Fig. 3 (a) DSC thermograms. (b) The dependence of the T_g of samples on the ratio of the VSD and CO. Thermogravimetric analysis (c) TGA and (d) DTG curves.

castor oil increased to 30%, the T_g of samples showed a nearly linear gradual increase from 18.4 to 70.9 °C (Fig. 3b). We speculated that the introduction of small molecules resulted in a decrease in the free volume of polymer molecular chains, which was the main reason for the increase in the T_g of segments. Besides, due to the presence of a rigid benzene ring in VSD, the mobility of network chains was further limited. All these films exhibited similar thermal degradation profiles, as shown in Fig. 3c and d. In the initial thermal degradation stage (200–320 °C), the weight loss was caused by the dissociation of the unstable urethane bond. The further degradation in the temperature range of 350–450 °C was mainly attributed to the breakage of the polyol chains. However, after introducing rigid diol containing dynamic bonds, the 50 wt% weight loss temperature (T_{50}) of CWPU-VSD was higher than that of CWPU (343.6 °C), which suggested that the benzene ring structure improved the thermal stability of this molecular customized sample.

3.4. Self-repairing performance and reprocessability

The basic characterization of mechanical and thermophysical properties demonstrated the great potential of CWPU-VSD samples for meeting the application requirements. Subsequently, films (thickness of about 0.5 mm) were cut into two pieces and heated to 120 °C to examine their self-healing behavior, which was observed using an optical microscope. As illustrated in Fig. S4,† the scratch width progressively narrowed over time and completely disappeared after 30 min. The healed CWPU-VSD30 could be bent without breakage (Fig. 4a), while the scratch on CWPU was still clearly visible and could not be completely cured under the same conditions (Fig. 4b). To further evaluate the healing efficiency more accurately, we calculated the ratio of tensile strength and elongation at break before and after repair (Fig. 4c). With the increase of the content of acylhydrazone groups in the cross-linked network, the healing efficiency of the films correspondingly increased. Among them, CWPUs without a sufficient amount of dynamic bonds showed unsatisfactory mechanical properties upon thermal healing, whereas CWPU-VSD30 exhibited an excellent healing efficiencies of 93.6% and 90.1% for tensile strength and elongation at break.

Later on, we further explored the reprocessability of CWPU-VSD30 (Fig. S5a†). The film was ground into fragments and then remolded by hot pressing (5 MPa at 120 °C for 30 min) to obtain a coherent and smooth remolded film. The stress–strain curve of the remolded film was nearly identical to

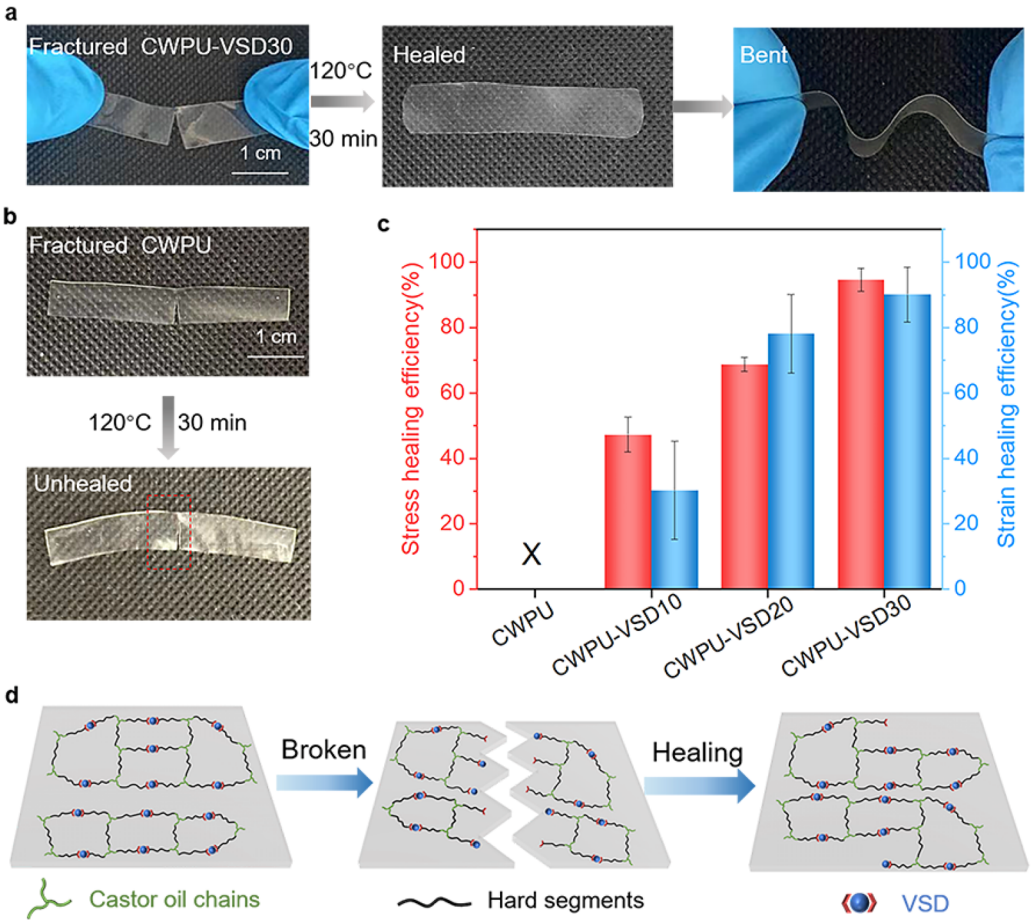

Fig. 4 (a) Photos of the self-healing behavior of the CWPU-VSD30 film. (b) Photos showing poor self-healing ability of CWPU. (c) The self-healing efficiency of tensile strength and strain. (d) The schematic diagram of the process of network reconstruction.

that of the original samples (Fig. S5b†), indicating excellent reprocessability and recyclability. The self-healing and reprocessing properties of the CWPU films could extend the service life of related products, thereby reducing plastic pollution and resource waste. In order to better understand its self-healing capability and recyclability, a schematic diagram of the molecular design strategy for this network recombination is shown in Fig. 4d. The exchange reaction of acylhydrazone bonds[33] in CWPU-VSD30 could transform the damaged cross-linking network structure into a new cross-linked network under external temperature stimuli.

3.5. Application as a multifunctional coating for paper substrates

The surface properties of CWPU series films were first investigated through a water contact angle (WCA) test and a water absorption test, which are usually the main indicators of water resistance. The WCA of the obtained film showed a slightly upward trend with the use of VSD diols (Fig. S6a†). Theoretically, partial substitution of hydrophobic CO by VSD would increase the hydrophilicity of the network, leading to a decrease in water contact angle. The increase in contact angle may be mainly attributed to the fact that a denser network was obtained with increasing diol content, which was evidenced by the swelling test (Fig. S6b†). Compared with the G_f (76.2%) of CWPU, the G_f of CWPU-VSD30 reached 89.7%, reflecting a higher degree of crosslinking. Fig. S6c† further showed that CWPU-VSD30 with higher crosslinking density could maintain its unchanged shape and appearance in water for 24 h, while the CWPU film turned white and curled. We hypothesized that water molecules were more likely to enter into the lower cross-linked networks and lead to swelling of the material, which was confirmed by the results of the sample water absorption experiment (Fig. S6d†).

Given the good water resistance and self-healing of CWPU-VSD30, its dispersion was tried as a multi-functional coating for paper substrates. To investigate the microstructures of papers coated with CWPU-VSD30, SEM analysis was performed and the results are shown in Fig. 3a–c. After coating, the porous fibrous structure of paper was completely covered by CWPU-VSD30, forming a dense and smooth film without any pinholes. This was attributed to the fact that the presence of multiple hydrogen bonds and high cross-linking density of the coating effectively reduced the pinholes caused by water

evaporation, which played a crucial role in improving the barrier properties of the coated paper.[34] The WCA of uncoated paper was 13.16°, and the WCA of the coated paper increased to 74.34°. Furthermore, the original water resistance of the scratched coated paper was restored after it was hot-pressed at 120 °C for 5 min, indicating good self-repairing capability of the coated paper. Subsequently, the water and water vapor resistance of coated papers were evaluated by testing their Cobb 60 value (an index to examine the water resistance) and water vapor transmission rates (WVTR). The Cobb 60 values of samples significantly decreased from 55.42 g m^{-2} (raw paper) to the range of 0.95–2.53 g m^{-2}, while the coating amount had less effect on the Cobb values (Fig. 5d). Therefore, the coated paper with a coating amount of 10 g m^{-2} was chosen to further test the WVTR. Both the polymer and the coated paper exhibited favorable results of 0.98 and 2.21 g mm m^{-2} day^{-1}, respectively, which were outstanding when compared to other common biopolymers[35,36] (Fig. 5e). Moreover, our castor-oil-based waterborne polyurethane coating also had significant environmental and barrier advantages over some biomass-based coatings in the literature (for details see Table S1†). To test the water/oil resistance of coated paper, we dripped water and oil onto the surface of the paper and kept it there for 5 min. The raw paper showed obvious watermarks and oil marks after removing the water and oil droplets, while no residues were observed on the coated paper (Fig. 5f). The unique combination of self-healing ability, excellent water and oil resistance and low WVTR made this coating strategy a more reliable and efficient alternative for paper package applications.

3.5. Biocompatibility, recyclability and degradability of the coated paper

To evaluate the potential health impacts of our coating materials, we chose mouse fibroblasts NIH/3T3 as the *in vitro* model.[37] The cytotoxicity of the coated paper was assessed by the viability of NIH/3T3 cells cultivated together with samples for 48 h. There were no significant differences between the sample and control groups and few dead cells were observed (Fig. S7†). After accurate statistics, the cell survival rate of the coated paper was as high as 98.1% (Fig. 6a), indicating that the coating is non-toxic to cells and has favorable biocompatibility.

Commercially, aluminum foils or plastics (*e.g.*, polypropylene and polyethylene) are often laminated to paper to prepare paper packaging materials with excellent water resistance. As a price, the resulting composites lose their recyclability and degradability. Herein, a closed-loop recycling path for our coated paper is demonstrated in Fig. 6b. Using the principles that acid can facilitate the hydrolysis of acylhydrazone bonds and small molecule alcohols promote the cleavage of amino acid esters,[38,39] the cross-linking network of the coating was disrupted in HCl/methanol (1/9) mixed solvents at 25 °C for 30 min, enabling the paper to be recycled. In addition, direct outdoor soil burial was performed to evaluate the biodegradability. It can be seen from Fig. 6c that the uncoated paper completely decomposed in soil within 50 d, while the coated paper degraded relatively slowly due to the presence of a dense surface coating. Ultimately, the mass loss rate of the coated paper reached 64.3% after 3 months of burial (Fig. 6d),

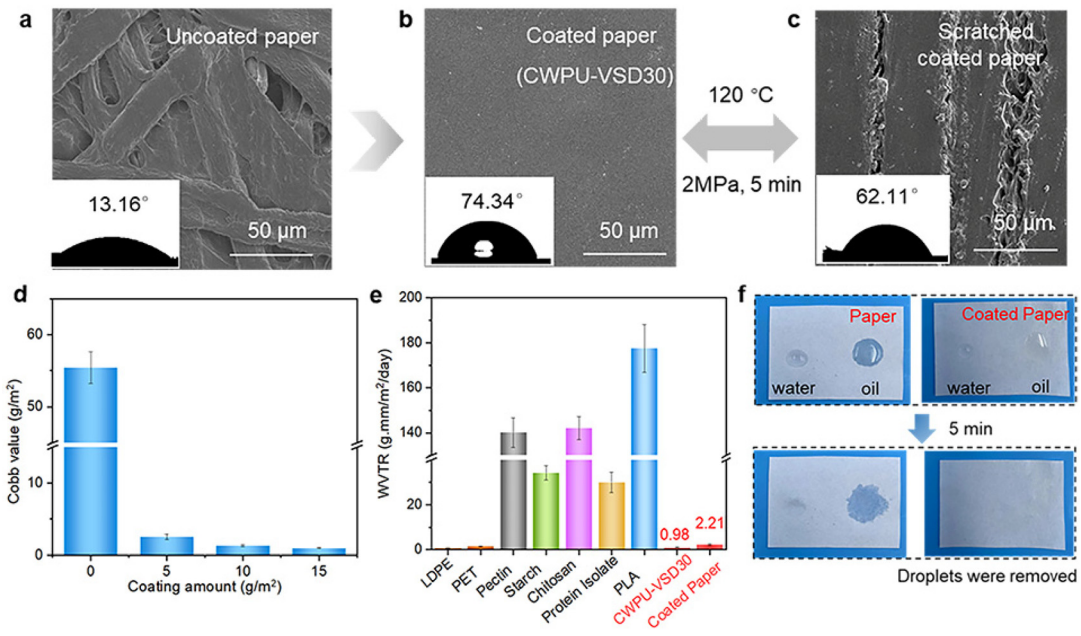

Fig. 5 (a–c) SEM images of raw paper, CWPU-VSD30 coated paper and scratched coated paper. Inset: water contact angle of samples (dwell time 120 s). (d) Cobb 60 values (g m^{-2}). (e) Comparison of the water vapor transmission rate (WVTR) of CWPU-VSD30 coated paper with common polymers used as coatings. (f) Behaviors of water and oil droplets on uncoated and coated paper within 5 min.

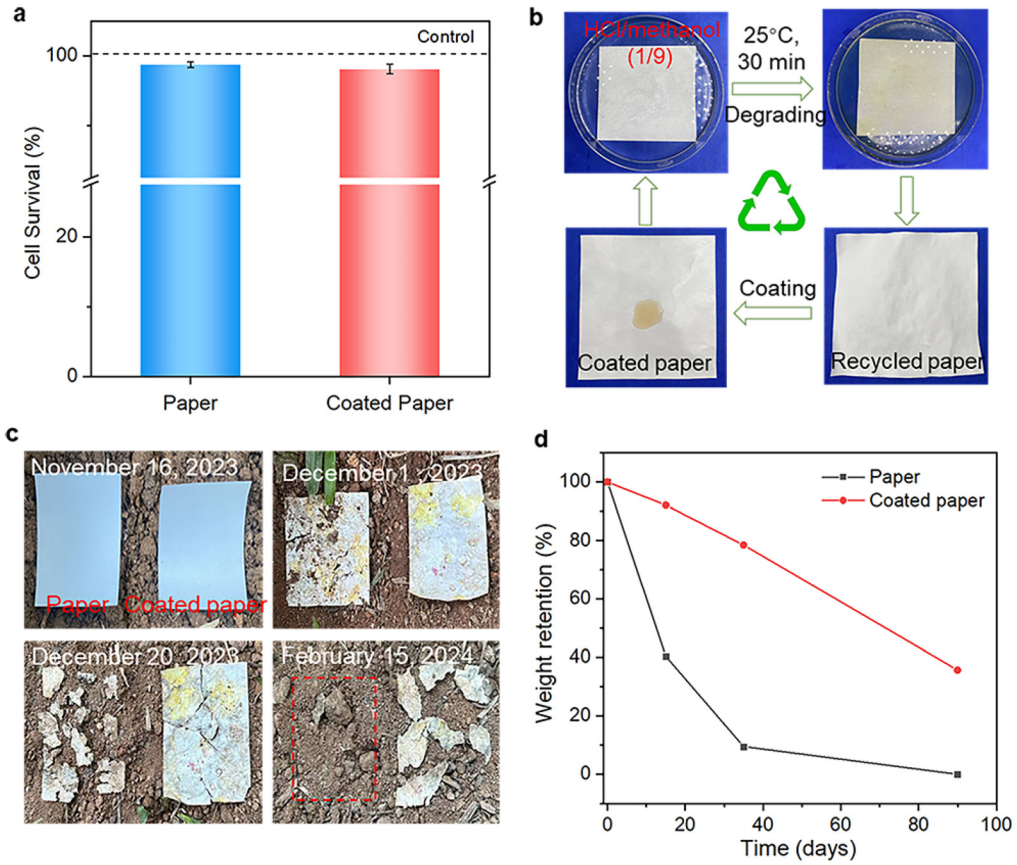

Fig. 6 (a) The survival percentage of NIH/3T3 cells in contact with the samples. (b) Closed-loop recycling process for our coated paper. (c) The degradation experiment of the paper and coated paper in natural soil. (d) The weight retention within 90 days.

demonstrating a promising biodegradation trend. The recyclability and biodegradability of the coated paper provide unique advantages over conventional paper–plastic or paper–aluminum composites.

4. Conclusion

In this work, a straightforward and effective strategy was developed to enhance both the mechanical properties and self-healing capability of castor oil-based WPU (CWPU) films. By introducing sustainable rigid diols (VSD) containing dynamic acylhydrazone bonds into the CWPU system, the film (CWPU-SVD30) demonstrated colorless transparency (with up to 90% transmission), high tensile strength (33.9 MPa) and impressive healing efficiency (>90%). Furthermore, the mechanical, thermophysical and water-resistance properties of the CWPU could be finely tuned by adjusting the ratios of VSD and castor oil. In addition, CWPU-VSD30 dispersion was first used as a functional coating for paper substrates. The results revealed that the coated paper had efficient excellent water- and oil-resistances, extremely low WVTR (2.21 g mm m^{-2} day^{-1}) and favorable biocompatibility, as well as good recyclability and biodegradability. These attributes provide a potential approach for developing multifunctional and sustainable paper-based barrier coatings.

Author contributions

Guowen Zhou: data curation, methodology, validation, investigation, visualisation, and writing – original draft. Yunfeng Zhou: investigation and methodology. Xiaoqian Zhang: validation and visualization. Zepeng Lei: resources, supervision, and writing – review & editing. Xiaohui Wang: resources, supervision, and writing – review & editing.

Data availability

The data that support the findings of this study are available from the corresponding author on reasonable request.

Conflicts of interest

The authors declare no competing financial interest or personal relationships that could have appeared to influence the work reported in this paper.

Acknowledgements

This work was supported by the National Natural Science Foundation of China (U23A6005, 32171721, and 22408111), the Guangdong Basic and Applied Basic Research Foundation (2023B1515040013 and 2023A1515110623), the Fundamental Research Funds for the Central Universities (2023ZYGXZR045 and 2023ZYGXZR093), and the State Key Laboratory of Pulp & Paper Engineering (2023ZD01, 2023C02).

References

1 A. Mouren and L. Averous, *Chem. Soc. Rev.*, 2023, **52**, 277–317.
2 L. Man, Y. Feng, Y. Hu, T. Yuan and Z. Yang, *J. Cleaner Prod.*, 2019, **241**, 118341.
3 S. Y. Kang, Z. Ji, L. F. Tseng, S. A. Turner, D. A. Villanueva, R. Johnson, A. Albano and R. Langer, *Adv. Mater.*, 2018, **30**, 1706237.
4 Y. Lu and R. C. Larock, *ChemSusChem*, 2019, **2**, 136–147.
5 J. Zhang, Y. Wu, H. Zhang, T. Yan, Y. Huang, J. Jiang and J. Tang, *Prog. Org. Coat.*, 2021, **157**, 106333.
6 C. Fu, Z. Zheng, Z. Yang, Y. Chen and L. Shen, *Prog. Org. Coat.*, 2014, **77**, 53–60.
7 C. Zhang, H. Liang, D. Liang, Z. Lin, Q. Chen, P. Feng and Q. Wang, *Angew. Chem., Int. Ed.*, 2021, **60**, 4289–4299.
8 R. Shen, C. Lei, M. Long, W. Gao, G. Yu and J. Tang, *Adv. Funct. Mater.*, 2023, **33**, 2212455.
9 H. Liang, Y. Li, S. Huang, K. Huang, X. Zeng, Q. Dong, C. Liu, P. Feng and C. Zhang, *ACS Sustainable Chem. Eng.*, 2020, **8**, 914–925.
10 R. Shen, M. Long, C. Lei, L. Dong, G. Yu and J. Tang, *Chem. Eng. J.*, 2022, **433**, 134470.
11 J. Shi, T. Zheng, Y. Zhang, B. Guo and J. Xu, *ACS Sustainable Chem. Eng.*, 2020, **8**, 1207–1218.
12 D. Xie, Y. Zhang, Y. Li, Y. Weng and J. Zeng, *Chem. Eng. J.*, 2022, **446**, 137071.
13 Y. Jin, Z. Lei, P. Taynton, S. Huang and W. Zhang, *Matter*, 2019, **1**, 1456–1493.
14 Z. Lei, H. Chen, S. Huang, L. J. Wayment, Q. Xu and W. Zhang, *Chem. Rev.*, 2024, **124**, 7829–7906.
15 Z. W. An, R. Xue, K. Ye, H. Zhao, Y. Liu, P. Li, Z. M. Chen, C. X. Huang and G. H. Hu, *Nanoscale*, 2023, **15**, 6505–6520.
16 F. Kong, X. Ma, X. Xu, M. Cui, H. Zhao, J. Zhu and J. Chen, *Mater. Today Chem.*, 2024, **35**, 101881.
17 W. Pu, D. Fu, Z. Wang, X. Gan, X. Lu, L. Yang and H. Xia, *Adv. Sci.*, 2018, **5**, 1800101.
18 S. Ji, W. Cao, Y. Yu and H. Xu, *Adv. Mater.*, 2015, **27**, 7740–7745.
19 K. Song, W. Ye, X. Gao, H. Fang, Y. Zhang, Q. Zhang, X. Li, S. Yang, H. Wei and Y. Ding, *Mater. Horiz.*, 2021, **8**, 216–223.
20 F. Song, Z. Li, P. Jia, M. Zhang, C. Bo, G. Feng, L. Hu and Y. Zhou, *J. Mater. Chem. A*, 2019, **7**, 13400–13410.
21 Y. Lei, Q. Chen, P. Liu, L. Wang, H. Wang, B. Li, X. Lu, Z. Chen, Y. Pan, F. Huang and H. Li, *Angew. Chem., Int. Ed.*, 2021, **60**, 4705–4711.
22 Y. Sun, D. Sheng, H. Wu, X. Tian, H. Xie, B. Shi, X. Liu and Y. Yang, *Polymer*, 2021, **233**, 124208.
23 X. Xu, X. Ma, M. Cui, H. Zhao, N. E. Stott, J. Zhu, N. Yan and J. Chen, *Chem. Eng. J.*, 2024, **479**, 147823–147832.
24 S. Lee, S. Shin and D. Lee, *Mater. Des.*, 2019, **172**, 107774–107784.
25 R. Xue, H. Zhao, Z. W. An, W. Wu, Y. Jiang, P. Li, C. X. Huang, D. Shi, R. Li, G. H. Hu and S. F. Wang, *ACS Nano*, 2023, **17**, 5653–5662.
26 X. Zhu, K. Han, C. Li, J. Wang, J. Yuan, Z. Pan and M. Pan, *ACS Appl. Mater. Interfaces*, 2023, **15**, 19414–19426.
27 W. G. Skene and J. Lehn, *Proc. Natl. Acad. Sci. U. S. A.*, 2004, **101**, 8270–8275.
28 R. Nguyen and I. Huc, *Chem. Commun.*, 2023, **8**, 942–943.
29 Q. Xing, P. Buono, D. Ruch, P. Dubois, L. Wu and W. J. Wang, *ACS Sustainable Chem. Eng.*, 2019, **7**, 4147–4157.
30 H. Liang, S. Wang, H. He, M. Wang, L. Liu, J. Lu, Y. Zhang and C. Zhang, *Ind. Crops Prod.*, 2018, **122**, 182–189.
31 Y. Zhang, Z. Wu, L. Shi, L. Dai, R. Liu, L. Zhang, B. Lyu, S. Zhao and V. K. Thakur, *Macromol. Mater. Eng.*, 2023, **308**, 2200662–2200672.
32 H. Deng, F. Xie, H. Shi, Y. Li, S. Liu and C. Zhang, *Chem. Eng. J.*, 2022, **446**, 137124.
33 N. Kuhl, S. Bode, R. K. Bose, J. Vitz, A. Seifert, S. Hoeppener, S. J. Garcia, S. Spange, S. van der Zwaag, M. D. Hager and U. S. Schubert, *Adv. Funct. Mater.*, 2015, **25**, 3295–3301.
34 J. Liu, Z. Tong, F. Gao, J. Wang, J. Hu, L. Song, Y. Hou, J. Lu, X. Zhan and Q. Zhang, *Adv. Mater.*, 2024, **36**, 2401982–2401995.
35 A. Sangroniz, J. B. Zhu, X. Tang, A. Etxeberria, E. Y. Chen and H. Sardon, *Nat. Commun.*, 2019, **10**, 3559–3566.
36 S. Jung, Y. Cui, M. Barnes, C. Satam, S. Zhang, R. A. Chowdhury, A. Adumbumkulath, O. Sahin, C. Miller, S. M. Sajadi, L. M. Sassi, Y. Ji, M. R. Bennett, M. Yu, J. Friguglietti, F. A. Merchant, R. Verduzco, S. Roy, R. Vajtai, J. C. Meredith, J. P. Youngblood, N. Koratkar, M. M. Rahman and P. M. Ajayan, *Adv. Mater.*, 2020, **32**, 1908291–1908300.
37 Y. Wang, X. Zhang, L. Kan, F. Shen, H. Ling and X. Wang, *Green Chem.*, 2022, **24**, 7039–7048.
38 X. Jiang, F. Zeng, X. Yang, C. Jian, L. Zhang, A. Yu and A. Lu, *Acta Biomater.*, 2022, **141**, 102–113.
39 Y. Sun, X. Tian, H. Xie, B. Shi, J. Zhong and X. Liu, *Polymer*, 2022, **258**, 125313–125322.